

Designs of porous polymer THz fibers

Alexandre Dupuis^a, Alireza Hassani^a, Maksim Skorobogatiy*^a

^aDept. of Physics Engineering, École Polytechnique de Montréal, C.P. 6079, succursale centre-ville
Montréal, Québec, Canada H3C 3A7

ABSTRACT

We propose various designs of porous polymer fibers for guiding terahertz radiation. Numerical simulations are presented for three fiber geometries: a Bragg fiber consisting of periodic multilayers of ferroelectric polyvinylidene fluoride (PVDF) and polycarbonate (PC), a sub-wavelength waveguide containing multiple sub-wavelength holes, as well as a cobweb-like porous Bragg fiber consisting of solid film layers suspended by a network of bridges. Various properties of these fibers are presented. Emphasis is put on the optimization of the geometries to increase the fraction of power guided in the air, thereby alleviating the effects of material absorption. Losses of about 10 dB/m, 7.8 dB/m, and 1.7 dB/m at 1 THz are respectively predicted for these three structures.

Keywords: Terahertz, Bragg fibers, polymer optical fiber

1. INTRODUCTION

Terahertz radiation, with wavelengths from 30 to 3000 microns, has big potential for applications such as biomedical sensing, noninvasive imaging and spectroscopy. On one hand, the rich spectrum of THz spectroscopy has allowed for the study and label-free detection of proteins¹, explosives², pharmaceutical drugs³, and the hybridization of DNA⁴. On the other hand, the substantial subsurface penetration of terahertz wavelengths has driven a large amount of work on THz imaging⁵. Applications range from non-destructive quality control of electronic circuits⁶ to the spatial mapping of specific organic compounds for security applications⁷. Although THz radiation is strongly absorbed by water, the combination of spectroscopy and imaging has been used to demonstrate the differentiation of biological tissues⁸. Terahertz sources are generally bulky and designing efficient THz waveguides, in order to remotely deliver the broadband THz radiation, would be a big step towards commercialization of compact and robust THz systems for these applications. However, almost all materials are highly absorbent in the THz region and there is also a large loss from the water vapor in the atmosphere. An efficient waveguide must therefore maximize the fraction of power guided in dry air, where the lowest absorption loss occurs. Before discussing the various porous waveguide designs that are presented here, let us begin with a review of the recent advances in THz waveguides.

1.1 Recent advances in metallic waveguides

Whereas the losses of circular metallic tubes⁹, like stainless steel hypodermic needles, have a propagation loss on the order of 5 dB/cm, recent techniques have considerably reduced the loss. On one hand, the use of thin metal layers on the inner surface of dielectric tubes¹⁰⁻¹², a technique which was initially developed for guiding CO₂ laser light, has been shown to successfully guide in the THz region. A thin Cu layer in a polystyrene tube¹⁰ and a thin Ag layer in a silica tube¹² have respectively been shown to have losses of 3.9 and 8.5 dB/m. On the other hand, surface plasmon mediated guidance on metallic wires has recently raised interest¹³ because of the lowest predicted propagation

*maksim.skorobogatiy@polymtl.ca; phone 1 514 340-4711 #3327; fax 1 514 340-3218; <http://www.photonics.phys.polymtl.ca>

losses¹⁴ of 0.9 dB/m. However, it is very difficult to excite the plasmons because their azimuthal polarization. Typical coupling losses are very high with less than 1% of the incident power transmitted; even with the development of specialized antennas only 50% coupling is achieved. Furthermore, the bending losses are very high and the surface plasmon is a very delocalized mode¹⁴. Since the mode extends many times the diameter of the wire into the ambient air, these waveguides have serious cross-talk issues with nearby metallic objects. For higher coupling efficiency, hollow core waveguides are preferable. As an additional advantage, hollow waveguides offer the possibility of putting an analyte directly into the waveguide core, thus dramatically increasing sensitivity of spectroscopy. Such porous structures are beginning to be studied for dielectric waveguides.

1.2 Recent advances in dielectric waveguides

Because of the high absorption losses in dielectrics, a variety of guiding mechanisms have been studied in order to reduce the propagation losses. On one hand, the resonance in the dielectric constant of ferroelectric polyvinylidene fluoride (PVDF) has been exploited for demonstrating a hollow core $n < 1$ waveguide¹⁵ with losses lower than 10 dB/m. However, PVDF is a semi-crystalline polymer that has many phases and a complicated poling procedure is required for achieving the ferroelectric state. On the other hand, different photonic crystal structures have been tried^{16,17}, but the absorption in a solid core remains considerable.

In yet another approach, many sub-wavelength waveguides have been developed¹⁸⁻²⁰. A solid sub-wavelength rod acts as a high refractive index core with the surrounding air acting as a lower refractive index cladding. The field of the guided mode extends far into the surrounding air resulting in low absorption loss. It is interesting to note that Nagel et al.²⁰ have shown that the addition of a sub-wavelength hole within the sub-wavelength core increases the guided field within the air hole, further reducing the losses. While current losses in dielectric waveguides are higher than those in metallic waveguides, there is reason to believe that a proper porous geometry could greatly reduce the losses.

1.3 Proposed porous waveguides

In order to take advantage of the high coupling efficiency of hollow core waveguides, we propose three designs of highly porous waveguiding structures that rely on different guiding mechanisms. The geometries of these structures are optimized to increase the fraction of power guided in the air, thereby reducing the absorption losses. The rest of the paper is organized as follows. In section 2, we present the design of a Bragg fiber consisting of periodic multilayers of ferroelectric polyvinylidene fluoride (PVDF) and polycarbonate (PC). We show that different guiding mechanisms come into play at different frequencies in the THz regime. Section 3 presents a sub-wavelength waveguide containing multiple sub-wavelength holes. The presence of multiple sub-wavelength holes extends an idea originally demonstrated by Nagel et al.²⁰, further increasing the fraction of power guided in the air. Section 4 presents a Bragg fiber with porous layers. A network of bridges supports solid film layers, forming a cobweb-like structure. Such a structure was initially proposed by Yu et al.²¹. Finally, the theoretical results are summarized in section 5.

2. FERROELECTRIC BRAGG FIBER

Hidaka et al.¹⁵ have demonstrated that when a layer of ferroelectric PVDF polymer is placed on the inside of a plastic tube, the resulting structure presents an efficient THz waveguide. Detailed analysis shows that PVDF polymer exhibits efficient metal-like reflectivity and considerably lower

absorption losses, compared to those of metals in the vicinity of 1 THz. We now demonstrate theoretically that a hollow core Bragg fiber (Fig. 1.a), featuring a reflector containing periodic layers of ferroelectric PVDF and a low loss polymer (PC), may be designed to exhibit large THz bandgaps²², near the transverse optical frequency of PVDF. We find that, depending upon the frequency of operation, the lowest loss hollow Bragg fiber can be one of the following: a photonic crystal fiber guiding in a band gap regime, a metamaterial fiber with a sub-wavelength reflector period, a single PC tube of a specific thickness, or a single PVDF tube of any thickness.

2.1 Analysis of planar multilayer stack

Confinement in this Bragg fiber is provided by the reflector, consisting of a periodic sequence of PVDF and PC layers of thicknesses d_{PVDF} and d_{PC} , with a PVDF layer closest to the core. We assume the hollow core diameter to be significantly larger than the wavelength of the transmitted radiation. Light propagation in such fibers may be seen as a sequence of consecutive reflections, at grazing angles of incidence, from an almost planar reflector (Fig. 2, $\theta \sim 90^\circ$).

In the THz region, the PVDF dielectric function exhibits a resonance:

$$\varepsilon_{\text{PVDF}}(\omega) = \varepsilon_{\text{opt}} + \frac{(\varepsilon_{\text{dc}} - \varepsilon_{\text{opt}})\omega_{\text{TO}}^2}{\omega_{\text{TO}}^2 - \omega^2 + i\gamma\omega}, \quad (1)$$

where the parameters are¹⁵ $\varepsilon_{\text{opt}} = 2.0$, $\varepsilon_{\text{dc}} = 50.0$, $\omega_{\text{TO}} = 0.3$ THz, $\gamma = 0.1$ THz. In comparison with PVDF, the dielectric response of PC polymer is frequency independent, having a purely real dielectric constant $\varepsilon_{\text{PC}} = 2.56$. The material in the core is air, with $\varepsilon_{\text{core}} = 1.0$. In the limit when material losses are negligible and the number of reflector periods is infinite, the theory of planar periodic reflectors²³ predicts that for a given angle of incidence θ onto such a reflector there exists a wavelength λ_c for which radiation of any polarization is reflected completely. Defining the modal effective refractive index as $n_{\text{eff}} = n_c \sin \theta$, while $\tilde{n}_{\text{PVDF}} = \sqrt{n_{\text{PVDF}}^2 - n_{\text{eff}}^2}$, and $\tilde{n}_{\text{PC}} = \sqrt{n_{\text{PC}}^2 - n_{\text{eff}}^2}$, then $\lambda_c / 2 = d_{\text{PVDF}} \tilde{n}_{\text{PVDF}} + d_{\text{PC}} \tilde{n}_{\text{PC}}$. Around λ_c , there exists a wavelength range $\Delta\lambda$, called the bandgap, such that, for any wavelength inside of the bandgap, radiation is still completely reflected. The relative size of the bandgap is proportional to the relative index contrast in the reflector multilayer $\Delta\lambda / \lambda_c \sim |\tilde{n}_{\text{PVDF}} - \tilde{n}_{\text{PC}}| / \langle \tilde{n} \rangle$. Furthermore, the bandgap size is maximized for a so-called quarter-wave reflector, where $d_{\text{PVDF}} \tilde{n}_{\text{PVDF}} = d_{\text{PC}} \tilde{n}_{\text{PC}} = \lambda_c / 4$. Finally, the efficiency of a finite reflector correlates with the bandgap size of a corresponding infinite reflector.

The real and imaginary parts of the refractive indices of the PVDF/PC material combination are presented in Fig. 1.c). In the regions $\omega \leq 0.2$ THz, and $2.0 \leq \omega \leq 2.6$ THz, PVDF losses are small $\text{Im}(n) \ll \text{Re}(n)$, while the relative refractive index contrast is high > 0.3 , suggesting the possibility of designing an efficient periodic reflector featuring a large bandgap. In the region $2.0 \leq \omega \leq 2.6$ THz, the real part of the PVDF refractive index is smaller than that of air, resulting in total internal reflection from the multilayer interface. In Fig. 2 we show the loss per single reflection from the infinitely periodic reflector for the lossiest TM polarized plane wave (magnetic field parallel to the reflector interface). A grazing angle of incidence θ , is fixed and equal to 89° . For every frequency, the loss is presented in shades of gray (white - low loss, black - high loss) as a function of the reflector layer thicknesses.

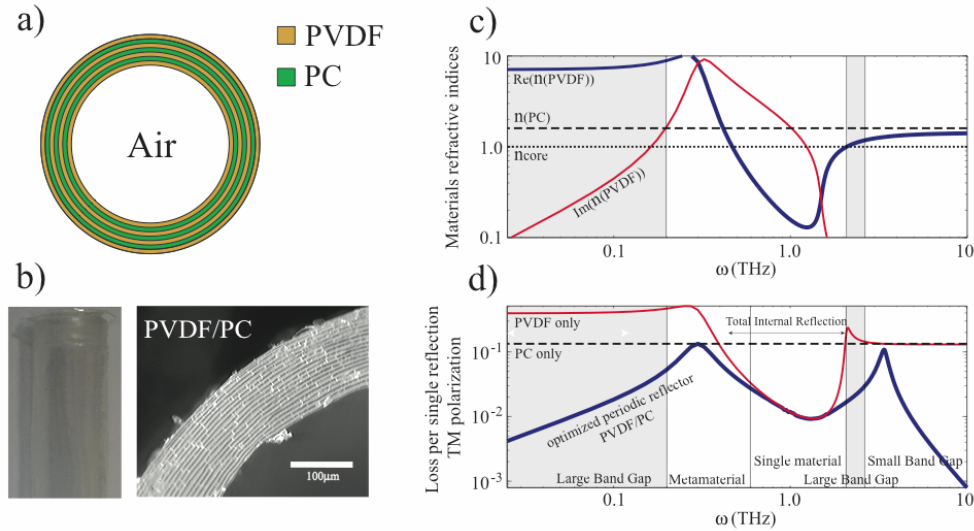


Fig. 1. (a) Theoretical cross-section of Bragg fiber. (b) Experimental cross-section of non-poled PVDF/PC Bragg fiber, fabricated by co-rolling method. (c) Re and Im parts of the reflector material refractive indices in terahertz. (d) Reflection efficiency from the semi-infinite PC (dotted line) and PVDF (thin line) layers, as well as from an optimized reflector (thick line).

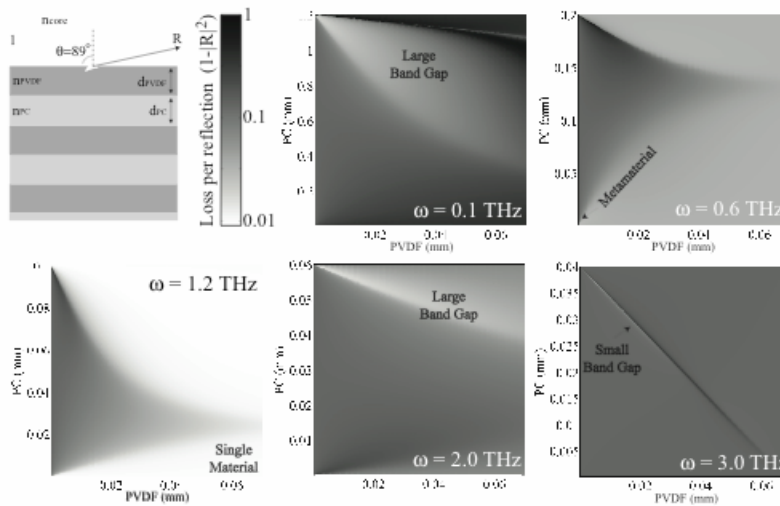


Fig. 2. Mapping of losses per single reflection from an infinite periodic reflector as a function of the layer thicknesses d_{PVDF} , d_{PC} , at various terahertz frequencies. $\theta = 89^\circ$.

As PC is assumed to be lossless, all the loss maps in Fig. 2 are periodic along the d_{PC} axis, where only one period is shown. For $\omega = 3$ THz and higher, due to small index contrast in a multilayer, the reflector bandgap is small and reflector efficiency is low. In this regime reflection from a periodic multilayer is similar to the reflection for a simple semi-infinite slab of some properly averaged dielectric constant. For $\omega = 0.1$ THz and $\omega = 2.0$ THz optimal reflectors have large bandgaps, as may be seen from the extended regions of phase space (d_{PVDF} , d_{PC}) characterized by high reflector efficiency (white regions in the corresponding figures of Fig. 2). In the region of total internal reflection (including $\omega = 1.2$ THz) we observe that reflection may be made very efficient simply by

using a thick enough PVDF layer. Finally, at lower frequencies $0.2 \leq \omega \leq 0.6$ THz PVDF absorption becomes very large; to minimize reflector loss a metamaterial in the form of a reflector with sub-wavelength period becomes most efficient. In this configuration, reflector losses are reduced below those of PVDF due to the presence of low loss PC, while metal-like PVDF provides efficient reflection.

To conclude our discussion of planar reflectors, in Fig. 1(d) we compare TM reflection efficiency from the optimized semi-infinite periodic PVDF/PC reflector (thick curve) with the reflection efficiencies from semi-infinite slabs of PVDF (thin curve) or PC (dotted curve). For a given frequency, the optimized reflector is found by first calculating a loss map (Fig. 2) of the reflector as a function of the PVDF and PC layer thicknesses, and then choosing the structure with the lowest loss. The optimal reflector guiding mechanism is indicated in Fig. 1(d) on the frequency axis. Note that reflection from a PVDF layer alone is very efficient in the frequency range of total internal reflection, when $\text{Re}(n_{\text{PVDF}}) < n_{\text{air}}$. However, beyond this region PVDF is highly absorbing and reflection from a single PC layer becomes more efficient. As periodic multilayers offer a possibility of bandgap guiding and metamaterial design, it is not surprising to find from Fig. 1(d) that optimal periodic PVDF/PC reflectors dramatically outperform single material reflectors. Finally, we note that at frequencies $\omega \sim 0.3, 3.4$ THz even the optimal reflectors become inefficient for the reflection of TM polarized waves. The nature of this anomaly is discussed elsewhere²³.

2.2 Analysis of Bragg fiber

We now present the theoretical transmission loss of the optimized 1 mm diameter hollow core Bragg fiber with a 31 layer PVDF/PC reflector, in Fig. 3. At all frequencies, the geometry of the optimal Bragg fiber is found by first constructing fiber loss maps (Fig. 3.a) and then choosing reflector layer thicknesses that minimize fiber transmission loss. We note that for the frequencies ~ 1 THz, individual reflector layer thicknesses are typically ~ 50 μm . At the fiber input we assume excitation with a Gaussian beam of 0.77 μm diameter, which empirically, gives the highest coupling efficiency (~ 90 - 98%) into the HE_{11} Gaussian-like core mode of a hollow fiber. To construct fiber loss maps (Fig. 3.a), for every choice of reflector layer thicknesses we first use the mode solver to find all the leaky and guided modes of the corresponding hollow Bragg fiber. Modal excitation coefficients are then found at the fiber input by expanding an incoming Gaussian beam into the fiber modal fields using the continuity of the transverse electromagnetic fields at the air-fiber interface. The excitation field is then propagated for 1 m. The remaining power at the fiber end is calculated, and the total loss is computed. In our simulations we find that the coupling loss is typically smaller than 0.5 dB, and the total loss of a fiber span is always dominated by the fiber loss. As discussed in the previous section, radiation propagation in the hollow core of a Bragg fiber can be thought of as a sequence of consecutive bounces from the confining reflector. Thus, the loss of a Bragg fiber is directly determined by the efficiency of a periodic reflector. Comparing loss maps of a planar multilayer (Fig. 3) with these of a Bragg fiber (Fig. 3.a)), it is not surprising to find that at the corresponding frequencies they look very much alike. Thus, optimal design strategies for the Bragg fiber reflectors are analogous to these for the planar reflectors. For example, in the frequency region 1.6-2.1 THz, refractive index contrast in a multilayer is high, while PVDF loss is relatively low. As a result, the optimal Bragg fiber is a bandgap guiding fiber. Finally, in the 1.0-3.0 THz region we show transmission loss (dots in Fig. 3.b) of optimally designed Bragg fibers and mark the guidance mechanisms. For comparison, we also present losses of a PVDF tube (dotted line in Fig. 3.b) of the

same bore radius and note that for frequencies higher than 1.6 THz, the optimally designed Bragg fiber considerably outperforms a PVDF tube.

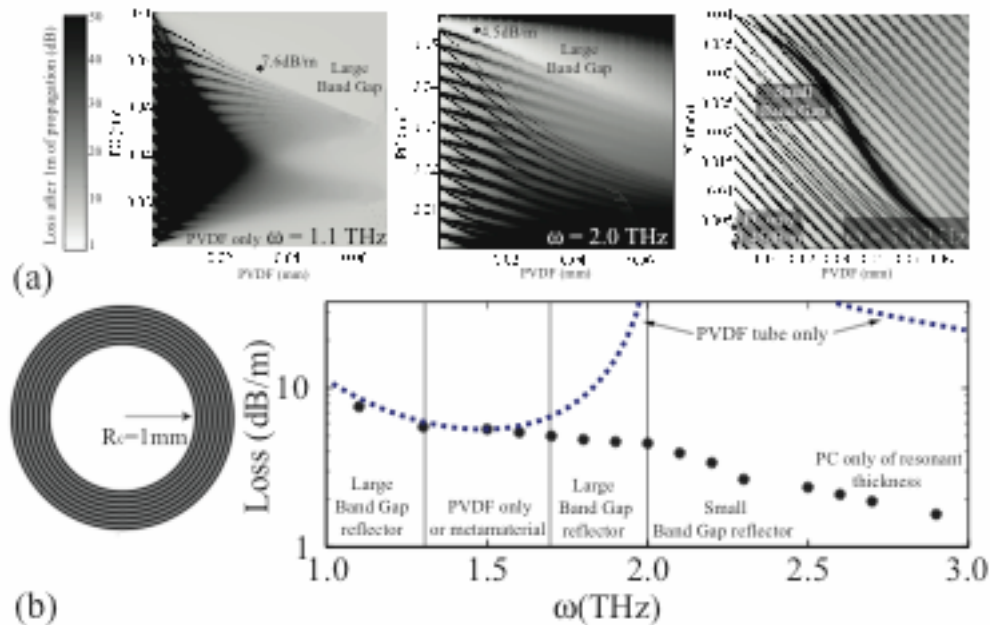


Fig. 3. (a) Mapping of the 1 mm core diameter hollow Bragg fiber transmission losses as a function of the reflector layer thicknesses at various THz frequencies. (b) Dots – transmission losses of the optimal hollow Bragg fiber designs. Dashed line – transmission loss of 1 mm core diameter PVDF tube guide.

3. SUB- λ WAVEGUIDE WITH MULTIPLE SUB- λ HOLES

For the second proposed fiber design, let us recall the low index discontinuity waveguide demonstrated by Nagel et al.²⁰ They considered a sub-wavelength air hole placed at the center of a glass rod. The glass acts as the core of this sub-wavelength waveguide, with the outside air acting as the low index cladding. However, due to the large refractive index difference between air and glass, a large discontinuity in the amplitude of the electrical field appears at the air-polymer interface, resulting in a proportionally high field concentration in the lower refractive index part (air hole). For a given refractive index material, it was shown that the sizes of the rod and the air hole can be optimized to maximize the concentration of THz power in the air hole.

This waveguide motivates us to design Multiple Sub-wavelength Hole THz Fiber (MSHTF), to further increase the fraction of power guided in the air. Figure 4 shows the schematic of the cross-section of our proposed microstructured THz fiber. The structure consists of a polymer rod having a hexagonal array of air holes. Let us emphasize that a periodic array of holes is not necessary as the guiding mechanism remains total internal reflection, not the photonic bandgap effect. For the polymer we assume a refractive index of 1.5, like the most polymers at 1 THz, and the refractive index of air is equal to 1. This fiber has 3 layers of holes and for the size of the holes we consider three different designs: $d = 0.1\lambda$, 0.15λ , and 0.2λ , where d is the hole diameter and λ is the operating wavelength. Furthermore, Λ indicates the pitch, or center-to-center distance between two holes, and the diameter of rod used in the simulations is 7Λ . The air hole size is fixed for each design and we reduce the pitch size, increasing the ratio d/Λ from 0.7 to 0.95, in order to study impact of the pitch

size on the fiber propagation features such as power confinement inside air holes, absorption loss and bending loss.

Figure 5.a) shows the effective index of the proposed fibers versus d/Λ for the three cases $d/\lambda = [0.1, 0.15, 0.20]$. Even though the refractive index of polymer is considered to be 1.5, the effective index of the fiber can reach below 1.05 by decreasing the pitch size to $\Lambda = d/0.95$ while the air hole size remains constant. As a result, the interaction between the THz waves and the absorptive polymer is greatly reduced. It is worth mentioning there is an optimum range for the hole size in order to confine as much power as possible inside them. Reducing the hole size less than 0.1λ or increasing it beyond 0.2λ decreases the capacity of the holes to confine the power. The appearance of an optimal size was found in the case of a single sub-wavelength air gap inside a silicon bulk or a glass rod waveguide²⁰.

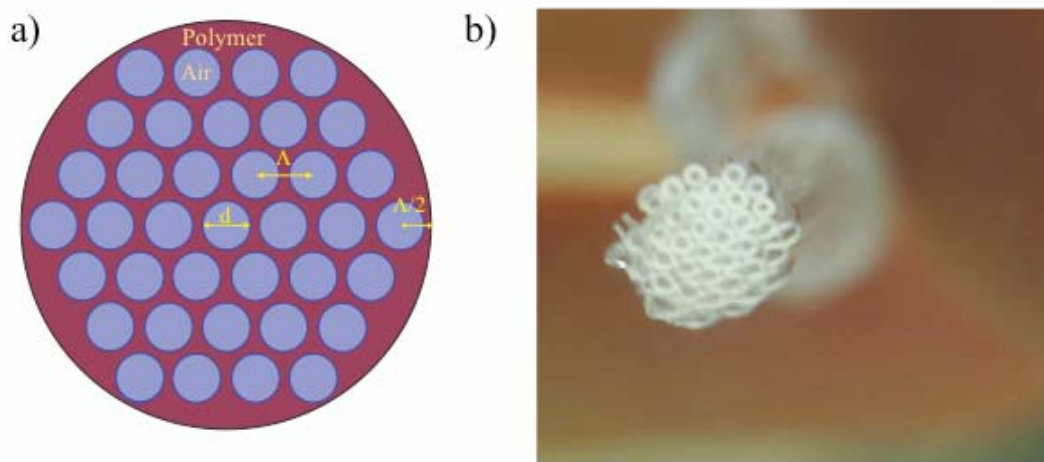


Fig. 4. a) Theoretical cross-section of sub-wavelength waveguide with multiple sub-wavelength holes. D is the diameter of the holes and Λ is the pitch. b) Experimental realization of a similar structure with an assembly of polymethyl methacrylate (PMMA) capillaries.

Another factor increasing the power confinement inside an air hole is the refractive index difference between the air and the material. Even though the polymer refractive index ($n=1.5$) is less than that of glass ($n=1.95$) and silicon²⁰ ($n=3.417$) at 1 THz, the presence of a multitude of holes in the proposed design increases the number of air regions where the THz radiation can be concentrated. Inset (a) and (b) in Fig. 5.a) show the S_z field distribution of the fiber with $d = 0.17 \lambda$ for the cases $\Lambda = d/0.75$ and $\Lambda = d/0.9$, respectively. First of all, in both cases the field distribution corresponds to the superposition of the Gaussian-like field distribution of a rod suspended in air, with an effective refractive index n_{eff} , and the field distribution of the individual sub-wavelength holes. Because of this, more power is concentrated in the air holes near the center of the fiber. Secondly, the pitch value of the first case is larger and the corresponding overlap between the field and the material is much larger than that of second case. Furthermore, the reduction of the fiber radius from 0.5 mm to 0.4 mm in the second case causes the field to extend farther outside of the fiber.

To obtain the fraction of the power propagating inside of air it is necessary to calculate the Pointing vector in the direction of propagation (S_z). The fraction of power guided in air then can be obtained by:

$$\eta = \frac{\int_{\text{air}} S_z dA}{\int_{\text{all}} S_z dA}, \quad (2)$$

where η is the power fraction, and "air" and "all" respectively indicate the air regions and the entire cross-section plane. Figure 5.b) shows the fraction of power with respect to d/Λ for the three fibers having different air hole sizes. The three upper lines show the total power fraction in the air while the three lower curves indicate the fraction of power that is contained solely within the air holes. For the case $d = 0.17\lambda$, as the pitch decreases the total power fraction in the air increases. This is also true for the power fraction in the air holes as long as $\Lambda \geq d/0.8$, otherwise the fraction of power decreases. The figure illustrates that for holes of $d = 0.1\lambda$ the optimum pitch for maximum power confinement is around $\Lambda = d/0.8$. Decreasing the pitch beyond that decreases the total power fraction in air due to the shrinking of the fiber radius which causes the escaping of the THz radiation from the air holes and the polymer to the air region outside of the fiber. It is worth mentioning that the diameter of the fiber can be calculated simply with $D=7[(d/\lambda)/(d/\Lambda)]\lambda$, and the smallest diameter, corresponding to $d = 0.1\lambda$ and $d/\Lambda = 0.95$, is 0.73λ indicating that the whole fiber can sometimes operate in the regime of a sub-wavelength waveguide¹⁹.

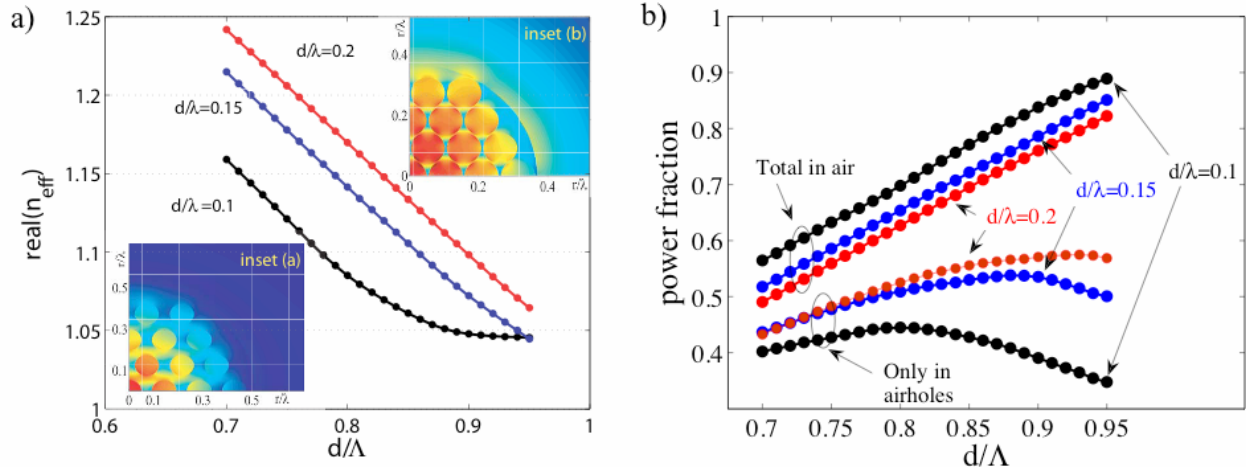


Fig. 5. a) The effective index of the fiber versus d/Λ for the three fiber designs having hole diameters of $d = 0.10\lambda$, 0.15λ , and 0.20λ respectively. For the fiber with $d/\lambda = 0.1$, inset (a) shows the S_z field distribution in the case where $\Lambda = d/0.75$ and inset (b) shows the S_z field distribution in the case where $\Lambda = d/0.9$. b) The power fraction guided by the fibers as a function of d/Λ . The three upper curves show the total power fraction in the air while the three lower curves indicate the power fraction in the holes only.

Focusing on the biggest pitch, $d/\Lambda = 0.7$, the bigger holes show more power confinement than the smallest holes. Moreover, the small power fraction differences between $d = 0.15\lambda$ and $d = 0.2\lambda$ indicates an upper limit to the power fraction in terms of optimization of the air hole size. Note that for these two cases, the maximum power fraction in the air holes will respectively occur at $d/\Lambda = 0.88$ and $d/\Lambda = 0.94$, which demonstrates the optimal fraction of power within the holes depend on the pitch size.

To calculate the modal absorption loss of the fiber, as a result of material absorption, we calculate the following fraction corresponding to the loss of the waveguide normalized with respect to the material loss²⁴

$$f = \frac{\alpha_{\text{wg}}}{\alpha_{\text{mat}}} = \left[\left(\sqrt{\frac{\epsilon_0}{\mu_0}} \int n(r) |\mathbf{E}|^2 dA \right) / \text{Re} \left(\int_{\text{total}} \bar{\mathbf{E}} \times \bar{\mathbf{H}}^* \cdot \hat{\mathbf{z}} dA \right) \right], \quad (3)$$

where α_{wg} and α_{mat} are the absorption coefficients of the THz waveguide and the bulk material (polymer), respectively. $\bar{\mathbf{E}}$ and $\bar{\mathbf{H}}$ are respectively the electric and magnetic fields, and n_r is the real part of the refractive index of the absorbent material (polymer). Figure 6.a) presents the normalized absorption loss as a function of d/Λ . The $d/\lambda = 0.1$ case gives a minimum normalized absorption loss of about 0.06 as a result of having the higher power fraction in the air. Considering the absorption loss of a low-loss material such as Teflon¹⁷ (0.3 cm^{-1}), one can obtain a fiber absorption loss of 0.018 cm^{-1} for this case ($d/\Lambda = 0.95$). Note that even in the d/λ case the minimum of absorption loss would be 0.03 cm^{-1} which is among the current lowest loss THz waveguides.

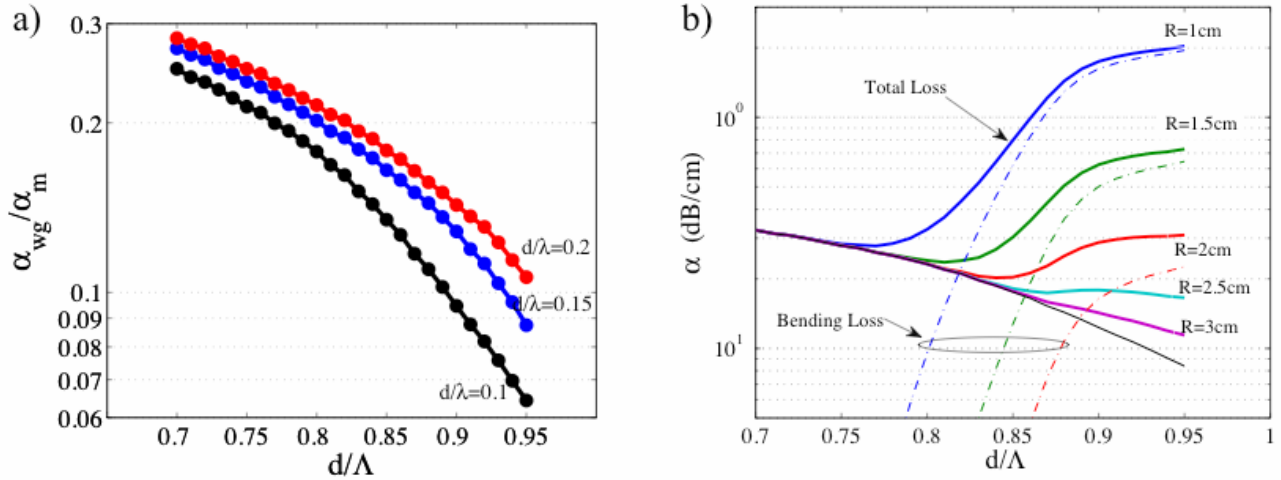


Fig. 6. a) Normalized absorption loss coefficient versus d/Λ for the three proposed fibers. b) Combination of bending and absorption loss versus d/Λ for the proposed THz fiber with $d/\Lambda = 0.1$

Another important parameter to consider is the bending loss. Even though calculating the bending loss for this structure is not an easy task, by considering the THz fiber as a step index fiber, i.e. the rod as a core of index n_{eff} and the air as a cladding, one can approximate the bending loss by an analytical formula which is valid for step index fibers and even some microstructured fibers²⁵. Due to the existence of sub-wavelength air holes in the polymer rod, the refractive index of the core should be considered equal to the corresponding calculated effective index. The bending loss coefficient for this case can be obtained by²⁵

$$\alpha \cong \frac{1}{8} \sqrt{\frac{2\pi}{3}} \frac{1}{\beta} F \left(\frac{2}{3} R \frac{(\beta^2 - \beta_{\text{cl}}^2)^{3/2}}{\beta^2} \right), \quad (4)$$

where $F(x) = x^{-1/2} \exp(-x)$, the propagation constant β is defined by $\beta = 2\pi n_{\text{eff}}/\lambda$ and R is the bending radius. A_{eff} is the effective area defined by²⁶

$$A_{\text{eff}} = \left[\int I(r) r dr \right]^2 / \left[\int I^2(r) r dr \right], \quad (5)$$

where $I(r)$ is the field intensity distribution in cross-section of the fiber. For the fiber having $d/\lambda = 0.1$, figure 6.b) shows two types of loss curves versus d/Λ . The first set of curves only show the bending loss for R ranging from 1 to 2 cm (dotted lines). Note that the thin solid black curve corresponds to the fiber absorption loss. The second set of curves indicates the superposition of bending loss, for R ranging from 1 to 3 cm, and absorption loss (solid thick lines). We see that there is an optimum for the fiber at a tight bending condition. In the region between $d/\Lambda = 0.7$ and $d/\Lambda = 0.8$ the dominant loss mechanism is the absorption loss due to the field-material overlap, whereas from $d/\Lambda = 0.85$ to $d/\Lambda = 0.95$ the bending loss for the cases we present is the dominant loss mechanism due to the penetration of THz field outside of the polymer rod. Note that the confinement of a major part of the THz power in the air holes prevents the apparition of a large bending loss even in the case of a small bending radius.

4. POROUS BRAGG FIBER WITH NETWORK OF BRIDGES

As a final design, we present a porous Bragg fiber having air gaps formed by a network of bridges. This idea was initially proposed by Yu et al.²¹ A schematization of the cross-section is presented in figure 7.a).

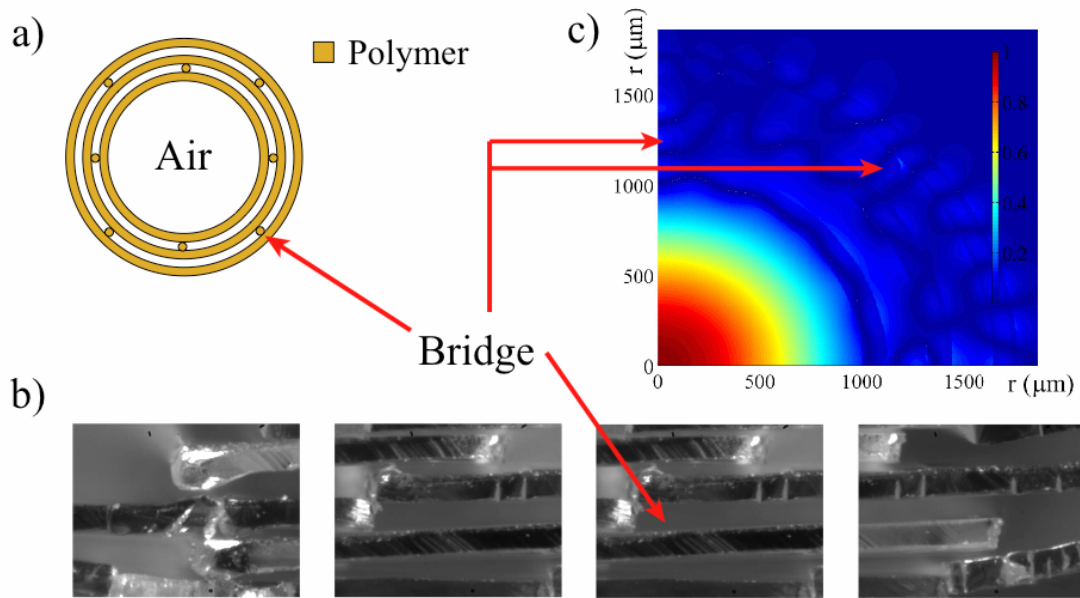


Fig. 7. a) Schematic of the cross-section used for the simulation. The porous Bragg fiber consists of solid polymer layers separated by a network of bridges, forming air gaps between the layers. b) Initial attempt at experimentally fabricating such a porous Bragg fiber by co-rolling a solid film with a second film having windows cut into it. The windows form the air gaps and the remaining polymer in the slotted film forms the bridges. c) S_z field distribution indicating that the field does not penetrate very far into the layers.

Since the bridges are small, the layers containing the bridges have an effective index close to that of air. Thus, the alternating layers of polymer and air yield a Bragg fiber with a high index contrast. Figure 7.b) presents optical microscope images showing the cross-section of an initial attempt at

making such porous Bragg fibers. The fiber was made by co-rolling a solid film with a second film that had windows cut into it. Once rolled, the windows formed the air gaps and the remaining bridges of the cut film formed spacers separating the solid film layers. Preliminary bolometer measurements of THz transmission through another type of similarly porous Bragg fiber lead us to roughly estimate the total loss to be around 42 dB/m. We are currently pursuing the transmission measurements of these fibers.

For the simulations, a polymer film thickness of 120 μm is considered. For simplicity, the bridges separating the solid layers are modeled by solid rods having a diameter of 100 μm . Fiber hollow core diameter is 2mm. The S_z field distribution of the lowest loss mode, calculated for the geometry in figure 7.a), is presented in figure 7.c). The field is mainly guided in the air core, with very little penetration into the reflector layers. Furthermore, figure 8 presents the real and imaginary parts of the refractive index for the lowest loss mode; the calculation was carried out in the same manner as that presented in section 2.2. The low loss regions ($\text{Im}(n_{\text{eff}})$ small) correspond to the bandgap regions of the Bragg fiber with theoretical radiation loss as small as 1.7dB/m at $\lambda=330\mu\text{m}$. Due to the presence of dielectric bridges, some of the bandgaps are further fractured by the surface states localized at the bridges positions.

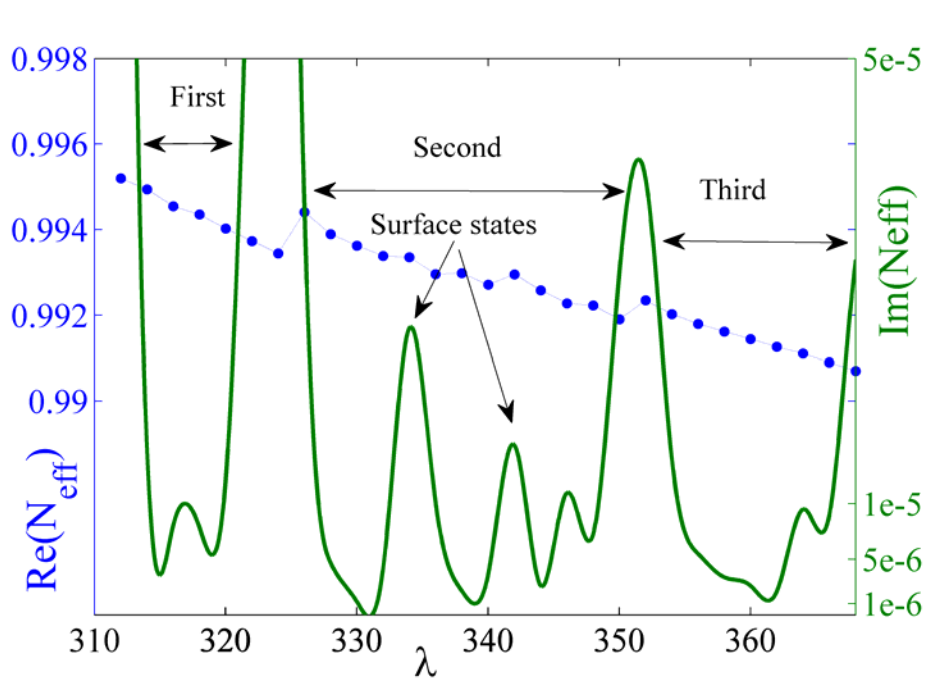


Fig. 8. Real and imaginary parts of the effective index of the lowest loss guided mode as a function of wavelength. The low loss regions ($\text{Im}(n_{\text{eff}})$ small) correspond to the bandgap regions of the Bragg fiber.

5. CONCLUSION

To summarize, we have started with an idea that near the transverse optical frequency of a ferroelectric polymer, a tube made of such a material can be used as an efficient hollow core THz waveguide. We then extended this idea to introduce a hollow core Bragg fiber with a periodic reflector containing ferroelectric polymer as one of its layers. Finally, we have demonstrated that a hollow Bragg fiber with an optimally designed reflector greatly outperforms a ferroelectric tube

guide. Moreover, depending upon the frequency of operation, the lowest loss Bragg fiber may have a bandgap, may have a metamaterial or simply a single material reflector.

Alternatively, we have proposed a microstructured polymer THz fiber composed of a polymer rod containing hexagonal array of subwavelength air holes. Let us emphasize that a periodic array of holes is not necessary as the guiding mechanism remains total internal reflection, not the photonic bandgap effect. The major portion of THz power launched into the fiber propagates inside of the air holes and the air surrounding the fiber. As a result, an absorption loss as low as 0.018 cm^{-1} can be achieved. Using an approximate analytical expression to calculate the bending loss of the fiber, we conclude that the presence of subwavelength holes as a THz power confiner reduces the large bending loss that normally accompanies a small bending radius.

Finally, we proposed a third design consisting of a Bragg fiber with porous layers. A network of bridges form air gaps between solid films layers. Even with the presence of bridges one can clearly observe the bandgaps, however fractured with occasional surface states. Inside of the bandgaps, modal fields are localized predominantly inside of the hollow fiber core. Theoretical radiation confinement loss is estimated to be as low as 1.7dB/m.

REFERENCES

- ¹ J. Xu, K. W. Plaxco, S. J. Allen, "Probing the collective vibrational dynamics of a protein in liquid water by terahertz absorption spectroscopy", *Protein Science*, **15**, 1175–1181, (2006).
- ² D. J. Cook, B. K. Decker, M. G. Allen, "Quantitative THz Spectroscopy of Explosive Materials", OSA conf.: Optical Terahertz Science and Technology 2005, PSI-SR-1196 (2005).
- ³ C. J. Strachan, P. F. Taday, D. A. Newnham, K. C. Gordon, J. A. Zeitler, M. Pepper, T. Rades, "Using Terahertz Pulsed Spectroscopy to Quantify Pharmaceutical Polymorphism and Crystallinity", *Journal of Pharmaceutical Sciences*, **94(4)**, 837-846 (2005).
- ⁴ M. Nagel, P. Haring Bolivar, M. Brucherseifer, H. Kurz, A. Bosserhoff, R. Büttner, "Integrated THz technology for label-free genetic diagnostics", *Appl. Phys. Lett.*, **80(1)**, 154-156 (2002).
- ⁵ W. L. Chan, J. Deibel, D. M. Mittleman, "Imaging with terahertz radiation", *Rep. Prog. Phys.*, **70**, 1325–1379 (2007).
- ⁶ T. Kiwa, M. Tonouchi, M. Yamashita, and K. Kawase, "Laser terahertz-emission microscope for inspecting electrical faults in integrated circuits", *Opt. Lett.* **28**, 2058-2060 (2003).
- ⁷ K. Kawase, Y. Ogawa, Y. Watanabe, H. Inoue, "Non-destructive terahertz imaging of illicit drugs using spectral fingerprints", *Opt. Express*, **11(20)**, 2549-2554 (2003).
- ⁸ T. Löffler, T. Bauer, K. J. Siebert, H. G. Roskos, A. Fitzgerald, S. Czasch, "Terahertz dark-field imaging of biomedical tissue", *Opt. Express*, **9(12)**, 616-621, (2001).
- ⁹ G. Gallot, S.P. Jamison, R.W. McGowan, D. Grischowsky, "Terahertz waveguides", *J. Opt. Soc. Am. B*, **17**, 851-863 (2000).
- ¹⁰ J. A. Harrington, R. George, P. Pedersen, E. Mueller, "Hollow polycarbonate waveguides with inner Cu coatings for delivery of terahertz radiation", *Opt. Express*, **12(21)**, 5263-5268 (2004).
- ¹¹ C. Themistos, B.M.A. Rahman, M. Rajarajan, K.T.V. Grattan, B. Bowden, J. A. Harrington, "Characterization of silver/polystyrene (PS)-coated hollow glass waveguides at THz frequency", *J. Lightwave Technol.*, **25(9)**, 2456-2462, (2007).
- ¹² C. T. Ito, Y. Matsuura, M. Miyagi, H. Minamide, H. Ito, "Flexible terahertz fiber optics with low bend-induced losses", *J. Opt. Soc. Am. B*, **24(5)**, 1230–1235 (2007).
- ¹³ K. Wang, D.M. Mittleman, "Metal wires for terahertz wave guiding", *Nature*, **432**, 376-379 (2004).

- ¹⁴ Q. Cao, J. Jahns "Azimuthally polarized surface plasmons as effective terahertz waveguides", *Opt. Express*, **13(2)**, 511-518 (2005).
- ¹⁵ T. Hidaka, H. Minamide, H. Ito, J. Nishizawa, K. Tamura, S. Ichikawa, "Ferroelectric PVDF cladding terahertz waveguide", *J. Lightwave Technol.*, **23(8)**, 2469-2473 (2005).
- ¹⁶ H. Park, M. Cho, J. Kim, H. Han, "Terahertz pulse transmission in plastic photonic crystal fibres", *Phys. Med. Biol.*, **43**, 3765-3769 (2002).
- ¹⁷ M. Goto, A. Quema, H. Takahashi, S. Ono, N. Sarukura, "Teflon photonic crystal fiber as terahertz waveguide", *Jap. J. Appl. Phys.*, **43(2B)**, L317-L319 (2004).
- ¹⁸ S.P. Jamison, R.W. McGowan, D. Grischkowsky, "Single-mode waveguide propagation and reshaping of sub-ps terahertz pulses in sapphire fibers", *Appl. Phys. Lett.*, **76(15)**, 1987-1989 (2000).
- ¹⁹ L.-J. Chen, H.-W. Chen, T.-F. Kao, J.-Y. Lu, C.-K. Sun, "Low-loss subwavelength plastic fiber for terahertz waveguiding", *Opt. Lett.*, **31(3)**, 306-308 (2006).
- ²⁰ M. Nagel, A. Marchewka, H. Kurz, "Low-index discontinuity terahertz waveguides", *Opt. Express*, **14(21)**, 9944-9954 (2006).
- ²¹ R.-J. Yu, Y.-Q. Zhang, B. Zhang, C.-R. Wang, C.-Q. Wu, "New cobweb-structure hollow Bragg optical fibers", *Optoelectronics Letters*, **3(1)**, 10-13 (2007).
- ²² M. Skorobogatiy, A. Dupuis, "Ferroelectric all-polymer hollow Bragg fibers for terahertz guidance", *Appl. Phys. Lett.*, **90**, 113514 (2007).
- ²³ M. Skorobogatiy, "Efficient anti-guiding of TE and TM polarizations in low index core waveguides without the need of omnidirectional reflector", *Opt. Lett.*, **30**, 2991-2993 (2005).
- ²⁴ A. W. Snyder and J. D. Love, "Optical Waveguide Theory", Chapman Hall, New York, (1983).
- ²⁵ M. D. Nielsen, N. A. Mortensen, M. Albertsen, J. R. Folkenberg, A. Bjarklev, D. Bonacinni, *Opt. Express*, **12**, 1775, (2004).
- ²⁶ N. A. Mortensen, *Opt. Express*, **10**, 341-348 (2002).